

Femtosecond fiber laser welding of dissimilar metals

Huan Huang,* Lih-Mei Yang, Shuang Bai, and Jian Liu

PolarOnyx, Inc., 2526 Qume Drive, Suite 17 & 18, San Jose, California 94538, USA

*Corresponding author: hhuang@polaronyx.com

Received 9 July 2014; accepted 22 August 2014;
posted 29 August 2014 (Doc. ID 216677); published 30 September 2014

In this paper, welding of dissimilar metals was demonstrated for the first time, to the best of our knowledge, by using a high-energy high-repetition-rate femtosecond fiber laser. Metallurgical and mechanical properties were investigated and analyzed under various processing parameters (pulse energy, repetition rate, and welding speed). Results showed that the formation of intermetallic brittle phases and welding defects could be effectively reduced. Strong welding quality with more than 210 MPa tensile strength for stainless steel–aluminum and 175 MPa tensile strength for stainless steel–magnesium has been demonstrated. A minimal heat affected zone and uniform and homogenous phase transformation in the welding region have been demonstrated. This laser-welding technique can be extended for various applications in semiconductor, automobile, aerospace, and biomedical industries. © 2014 Optical Society of America

OCIS codes: (060.3510) Lasers, fiber; (300.6365) Spectroscopy, laser induced breakdown; (140.3390) Laser materials processing.

<http://dx.doi.org/10.1364/AO.53.006569>

1. Introduction

Recently, dissimilar material welding has attracted high demand in automobile, aerospace, and biomedical applications. For example, automobile industries are choosing new materials to reduce weight, save cost, and make cars more energy saving and environmentally friendly. Aluminum (Al) alloys and new low-weight steels are now the standard car materials for engine blocks and wheels. Magnesium (Mg) alloys are in the implementation stage to further reduce weight by 50%. These new materials bring challenges for automobile manufacturing in material joining techniques, especially for joining dissimilar materials. The main challenges are thermal expansion mismatch due to the difference in the thermal expansion coefficient and the melting temperature of dissimilar materials, reduced temperature and load ranges due to the crack and residual welding stress, and increased directionality due to the formation of unstable intermetallic phases.

Current laser joining uses continuous-wave (CW) or long-pulsed lasers, which require high power input. The difference in the thermal expansion coefficients of the materials causes thermo-mechanical stress in both materials, so the joint is not strong enough. High power induced thermal diffusion outside the focal volume can cause damage to the joint. Different approaches have been tested to restrict the formation of intermetallic phases, such as pre and postweld heat treatment [1–3], controlling the diffusion mechanism by applying a lower heat input [4], offsetting the laser beam and using a combination of a higher laser power/higher welding speed [5], or applying a backing block below welding samples to control the heat flow and suppress the thickness of the intermetallic layer in welding alloy [6]. However, these approaches cannot resolve all of the fundamental issues for dissimilar material welding. As an example, the melting temperatures are different for Al (~650°C) and steel (~1538°C). When welding the two materials, the Al will melt and flow away before the steel is melted. Use of an Al–steel transition insert may help, but it adds more complexity and cost to the welding process. Given these challenges, novel

processes must be conceived that can reduce the thermally melted joining, eliminate heat affected zone (HAZ), and restrict the formation of intermetallic phases at the same time.

Alternatively, femtosecond (fs) lasers have been widely used in many fields including laser microfabrication, laser surgery, and biomedical applications. The main characteristic of the fs laser pulse is a high peak intensity that results in rapid delivery of energy into the material, which is much faster than plasma expansion; therefore thermal damages are significantly reduced or eliminated. Femtosecond lasers have been demonstrated by many researchers for welding various glass, silicon, copper materials, and tissue [7–9]. Femtosecond-laser-based welding allows space-selective joining without inserting intermediate layers; the highly localized heat generation minimizes the thermally induced stress and effectively suppresses the development of thermally induced cracks. It also shows that high-repetition-rate laser systems operating in the megahertz range can lead to an enlarged modification region due to heat accumulation of successive pulses [10,11]. Compared with conventional laser joining techniques (thermally melted welding), fs laser welding offers many advantages including localized heating, a HAZ-free, stable submicrometer joining structure, and a stable phase structure. However, little experimental demonstration besides some theoretical works [12,13] has been published for fs laser welding of dissimilar metals.

In this paper, welding of dissimilar metals is reported for the first time, to the best of our knowledge, using a high-energy high-repetition-rate fs fiber laser. It is the enabling technology for automobile manufacturing to weld steel, Al, and Mg alloys with much stronger bonding compared with conventional methods. We have experimentally demonstrated the critical functions of fs fiber laser welding and achieved the world's first fs fiber laser-welding process, to our best knowledge. The fs laser-welding mechanisms are also discussed.

2. Experimental Setup and Materials

Figure 1 shows the experimental setup for high-repetition-rate fs fiber laser dissimilar metal welding

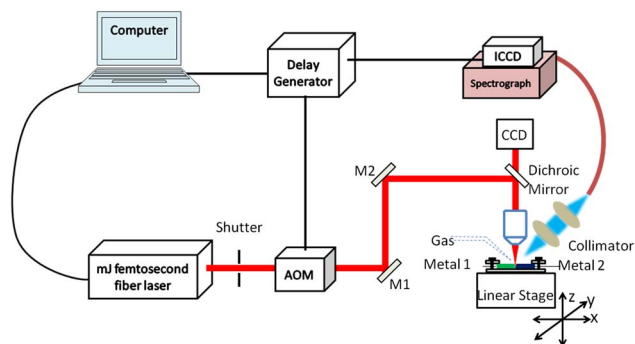


Fig. 1. Sketch of experimental setup for fs fiber laser metal welding.

in the application lab of PolarOnyx, Inc. It comprises a 0.5 mJ level fs fiber laser system, beam delivery components, an acousto-optic modulator (AOM), an automated three-dimensional motion system, a sample fixture, and a computer for system control. The fs fiber laser system is a commercialized high-energy mode-locked fiber laser (Uranus mJ series) manufactured by PolarOnyx Laser, Inc., and detailed information can be found from Ref. [14]. The output pulsewidth is 750 fs, and the repetition rate is tunable between 100 kHz and 10 MHz with an AOM. The laser beam wavelength is centered at 1030 nm. The maximum output pulse energy is 500 μ J at 100 kHz. The laser beam is reflected by mirrors and focused by a focusing lens ($f = 100$ mm) towards the sample on the sample fixture. The pulse energy is adjustable by the AOM, and a CCD camera is used to help laser beam alignment of the focus position. The motion system includes an automated high-accuracy three-dimensional linear stage. An ICCD with fiber and collimator for laser-induced breakdown spectroscopy (LIBS) signal collection is also added for laser-welding process monitoring and analysis.

Before bonding, each sample is polished especially on the edges so that the two edge surfaces have $\theta = 3^\circ$ of angle. Fixturing is extremely important, and the samples were clamped with the angled edge surface contacted at the bottom using a sample fixture, as shown in Fig. 2. Furthermore, the sample fixture has rotation and two tilt angle adjustments for sample tilting and alignment to the laser beam. The edge is aligned perfectly with the beam scanning direction with the help of a camera. The sample moves together with the linear stage, and the laser beam was focused at the center of the contacted sample gap and scanned along the contacting edges. During laser processing, no shielding gas was applied to the processing volume, and no filling material was added for welding.

The metal samples used in the experiment include Al alloy (Al3003), stainless steel (SST321), and Mg alloy (AZ61). Table 1 shows the chemical composition of the metal alloys used in the welding experiment. The two bonding samples have the same thickness (0.5 or 1 mm thick) and are precut to 1 in. \times 0.5 in. dimensions.

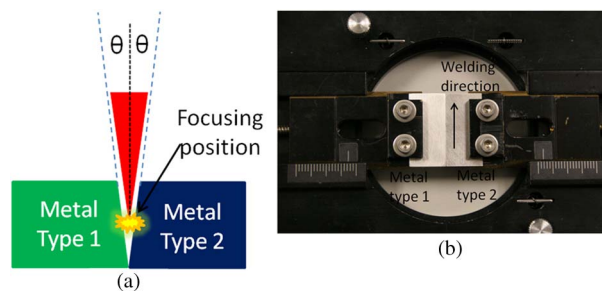


Fig. 2. (a) Sketch of polished sample edge and focusing position in the center of metal thickness. (b) Camera view of sample fixture for fs laser welding.

Table 1. Chemical Composition of Metal Alloys Used in the Welding Experiments

Alloy	Chemical Composition (wt. %)							
	Mn	Fe	Si	Cu	Cr	Zn	Zr	Al
Al3003	1.0–1.5	0–0.7	0–0.6	0–0.2	0–0.1	0–0.1	0–0.05	Balance
SST321	Cr	Ni	Mn	Si	Cu	C	Fe	Balance
	17–19	9–12	0–2	0–1	0–0.75	0–0.08		
AZ61	Al	Zn	Mn	Si	Fe	Mg	Balance	
	6.5	0.46	0.14	0.01	0.003			

After the welding, metallographic samples of the joints were cut perpendicularly to the welding direction and polished. The microtopography of the welding area was characterized with an upright digital microscope (Amscope, ME520T-9M). The welding shape, including the weld width and depth, was measured and analyzed by scanning electron microscopy (SEM) (FEI, QUANTA FEG 600) with an energy-dispersive x-ray (EDX) detector.

3. Experimental Results and Discussion

To systematically study dissimilar metal bonding using an fs fiber laser, different laser parameters and processing conditions were evaluated for the three metal alloys. A series of experiments was carried out to investigate the correlation of bonding quality with laser pulse energy, repetition rate, and welding speed.

A. Welding Results and Discussion

Figure 3 shows the camera view of the typical welded Al–SST sample. The laser parameters used include a 1 MHz repetition rate and 30 μJ pulse energy (30 W average power). No visible crack was observed near the sample welding position.

Figure 4 shows the SEM macrograph of a cross section of Al–SST welding results. The samples were processed by using different repetition rates (100 kHz, 500 kHz, 1 MHz, and 1.5 MHz) and the same average power –30 W. The processing speed is 1 mm/s.

When the repetition rate is very low (e.g., 100 kHz) and the pulse energy (e.g., 300 μJ) is very high, laser ablation dominates the process, which results in material removal [Fig. 4(a)]. The ablation plume

and debris are observed at the edge of the ablation area. Although welding occurs under the ablation area, the bonding is very weak and the undesirably large amount of material removal is detrimental to the original materials.

When the pulse energy is reduced to 60 μJ and the repetition rate is increased to 500 kHz, laser ablation is also observed but not dominant [Fig. 4(b)], successful welding is observed. When further increasing the repetition rate to 1 MHz and reducing the pulse energy to 30 μJ , ablation can still be seen since the pulse energy is still above the ablation threshold, but the material removal rate is smaller and the welding effect becomes dominant [Fig. 4(c)]. As the repetition rate is further increased to 1.5 MHz, the welding effect becomes even more dominant over the ablation [Fig. 4(d)].

Figure 5 summarizes the welding seam width measured at different distances to the top surfaces for different repetition rates and the same average power as shown in Fig. 4. At the same repetition rate, the welding seam width decreases (e.g., from 150 to 55 μm) as the distance to the surface increases (from 100 to 400 μm). With the increase of repetition rate (e.g., from 500 kHz to 1.5 MHz), the welding seam width increases (from 90 to 150 μm) at the same distance to the surface (100 μm deep). This is mainly due to plasma shielding and reflection. The higher the repetition rate, the shorter the time between two pulses. The laser energy can be scattered by the ablation plume and debris generated by previous pulses.

For the welding results using CW or nanosecond (ns) lasers from the literature [15–17], the welding region is in the millimeter range with a large amount of material experiencing melting and solidification. Furthermore, a large HAZ (hundreds of micrometers to millimeters) can be seen near the welding area. In contrast, as shown in Fig. 4, the HAZ is very limited by using an fs laser, and the material experiencing melting and solidification is less than 200 μm . This localized heat input is due to high peak intensity in the focal region that results in rapid delivery of energy into the material. Therefore, the thermal stress and thermally induced cracks are largely suppressed. The localized melting and welding is attributed to the melting pool near the focal region. Meanwhile, the large amount of pulse overlapping and heat accumulation helps to enlarge the melting pool, which provides more favorable conditions for fs laser welding. As stated and simulated in Ref. [12],

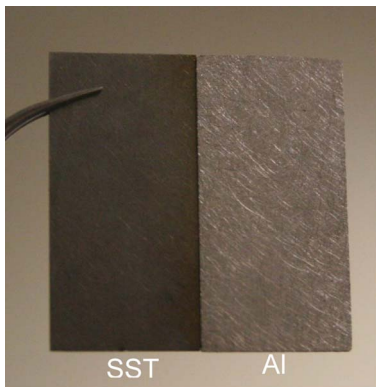


Fig. 3. Camera view of the welded Al–SST sample.

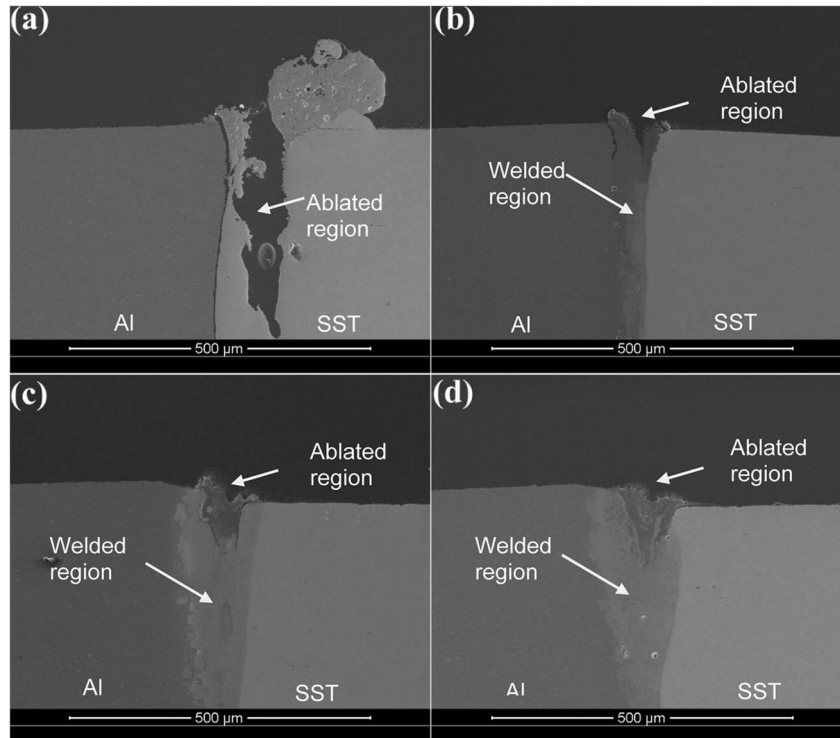


Fig. 4. SEM view of cross section of Al alloy and SST weld using fs fiber laser: (a) 100 kHz, 30 W; (b) 500 kHz, 30 W; (c) 1 MHz, 30 W; and (d) 1.5 MHz, 30 W.

only a limited amount of molten pool can be obtained from a single ultrashort laser pulse, regardless of input fluence. However, it is different for the multi-pulse and high-repetition-rate cases. The molten pool thickness after the second pulse is generally larger than after the first pulse. It is interesting to note that two pulses at high repetition rates result in more than two and a half times deeper molten pool thickness, suggesting that high repetition rate helps form a solid deep welding seam. It is summarized that the favorable conditions for fs laser welding is to use low fluence pulses with repetition rate in the order of

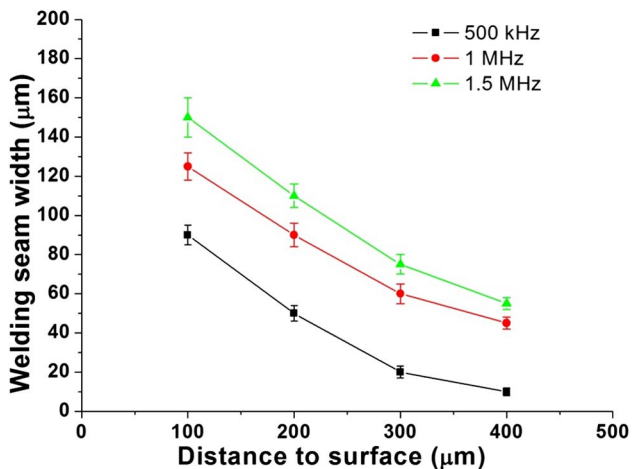


Fig. 5. Welding seam width at different distances to the surface at different repetition rates.

1–10 GHz [12]. This is consistent with the experiment results in this study, although the repetition rate was increased from 100 kHz to 1.5 MHz.

In order to understand the welding mechanism, the laser-welded zone between Al and SST metals was investigated. The cross-section SEM view at the focal position, the EDX line analytical results across the center of the welding zone, and the spot analytical results of the characteristic fusion zone were studied.

Figure 6 shows the SEM view of a cross section of Al–SST dissimilar welding (1.5 MHz and 30 W) with the EDX line and spot analytical region highlighted. Multiple EDX line profiles were acquired along three different depths (top, middle, and bottom) across the welding regions. Figure 6(b) shows a typical EDX line analytical result across the centerline of the welding region indicated in Fig. 6(a). The concentration change of different elements across the line is indicative of diffusion. Especially for the region from 50 to 100 μm, apparent mixing of nickel, iron, chromium, and Al can be seen, as shown in blue, cyan, green, and brown, respectively. Region 1 is pure Al alloy, and region 2 is pure SST. Other regions are near the central parts of the weld fusion zones.

Figures 7(a)–7(e) show the EDX spot analytical results of regions 1–5 in the cross-section view of Al–SST (1.5 MHz and 30 W) shown in Fig. 6(a). The element concentrations (both weight percentage and atomic percentage) are shown in the insets. All Al, Fe, Cr, and Ni existed in the weld fusion zones in regions 3–5. This slightly increases the

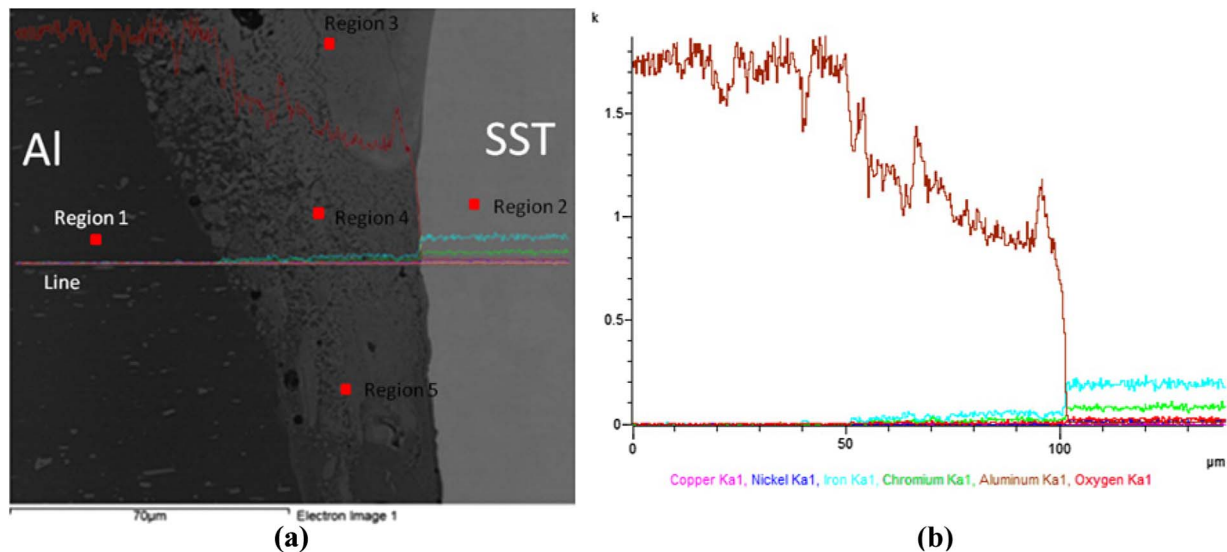


Fig. 6. (a) SEM view of cross section of Al alloy and SST dissimilar welding (1.5 MHz and 30 W) with EDX line and spot analytical region highlighted. (b) EDX line analytical results across the centerline of the welding beam.

concentrations of the displayed elements on the spot analytical region. Figure 7(a) shows EDX spot results for the pure Al alloy base metal (region 1). Figure 7(b) shows the EDX spot results for pure SST base metal with Cr, Fe, and Ni element constituents (Region 2). The EDX analysis results are consistent with the chemical composition of metal alloys used in the welding experiments. Figures 7(c) and 7(d) show the spot EDX analysis results near the central parts of the weld fusion zones. All Al, Fe, Cr, and Ni existed in the weld fusion zones of regions 3–5. Furthermore, the element concentrations vary slightly at these locations.

Figure 8 presents SEM micrographs showing microstructural changes of the Al alloy and SST joint by using fs fiber lasers with different repetition rates. The microstructure of the fs laser-welding zone is very fine, and the grain is in the range of 1–2 μm or even submicrometer level. Moreover, the grain size is very uniform across the welding region. This stable phase structure is formed with the localized ionization and heating by using an fs laser. However, the microstructure of the CW laser-welded zone is coarse, and the size is in the range of 20 μm or larger; the microstructure of the ns laser-welded zone is similar, and the size is also larger than the size by using an fs laser. Moreover the size distribution is not uniform in the region.

Grain refinement provides an important means to improve not only strength, but also ductility and toughness. When the grain size is reduced, there are more grains with a greater number of arbitrarily aligned slip planes for the dislocations in the grains. This provides more opportunity for some slip to occur in a stressed material. Fracture resistance is also improved with reduction in grain size, because the cracks formed during deformation, which are the precursors to those causing fracture, may initially be limited in size to the grain diameter. So this stable

micro and submicrometer structure and phase structure provides a unique foundation of better strength, ductility, and toughness, which is shown in the following mechanical testing results.

It is well known that Mg and steel are metallurgically incompatible due to their great differences in lattice type, lattice parameters, atomic radius, and electro-negativity. The big difference in melting point suggests that they cannot be melted simultaneously. In addition, the boiling point of Mg is only 1091°C, lower than the melting temperature of steel. This implies that molten steel will cause catastrophic vaporization of Mg if they come into contact with each other. With regard to their differences in metallurgical characteristics, Mg and Fe are immiscible and no intermediate phases can be produced according to the Mg–Fe binary diagram. Therefore, it is essential to add intermediate elements that can react with or possess substantial solid solubility in Mg and Fe [17,18].

Despite these challenges, by using the fs fiber laser, both Mg–SST and Mg–Al welding have been successfully achieved without adding intermediate fillers. Figure 9(a) shows a typical SEM view of a cross section of Mg–SST welding (1.5 MHz and 30 W) with the EDX line and spot analytical region highlighted. Region 1 is pure Mg alloy, and region 2 is pure SST. Other regions are near the central parts of the weld fusion zones. Similar to the welding of Al–SST, the HAZ is minimal. The material experiencing melting and solidification is even smaller, and an ultrathin welding region (<0.5 μm) was observed between the two metals. Figure 9(b) shows EDX line analytical results across the centerline of the welding region indicated in Fig. 9(a), and the concentration change of different elements across the line is indicative of diffusion. The mixing of Mg, iron, chromium, and nickel can be seen for the region from 12 to 16 μm, as shown in different colors.

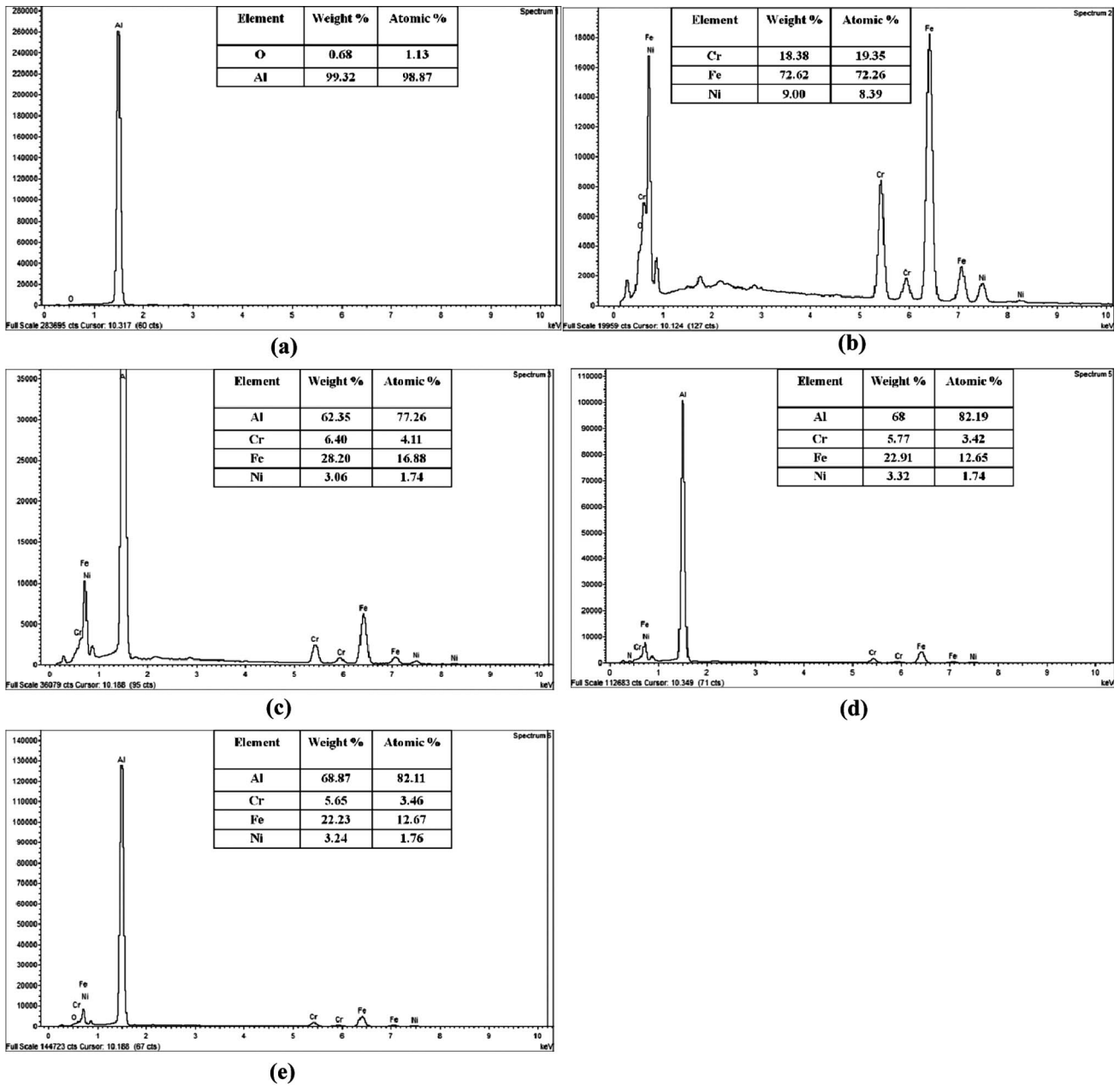


Fig. 7. EDX spot analytical results of different regions in the cross section view of Al-SST (1.5 MHz and 30 W) in Fig. 6(a): (a) region 1, pure Al alloy; (b) region 2, pure SST; (c) region 3; (d) region 4; and (e) region 5.

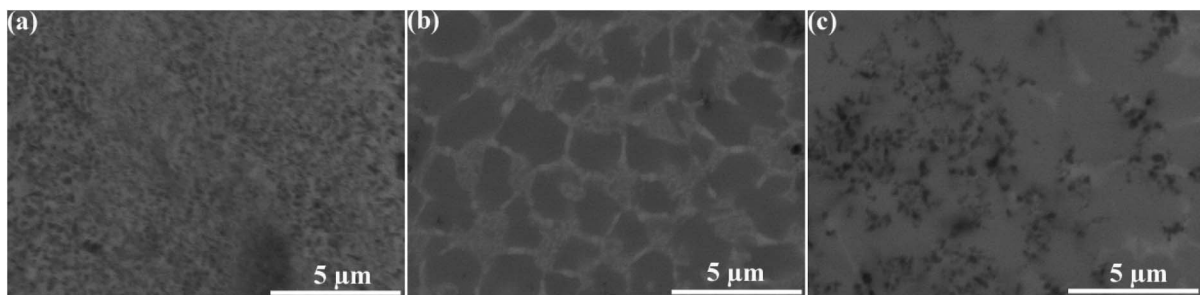


Fig. 8. SEM micrographs showing microstructure of Al-SST welded region using fs fiber laser with different repetition rates: (a) 500 kHz, 30 W; (b) 1 MHz, 30 W; and (c) 1.5 MHz, 30 W.

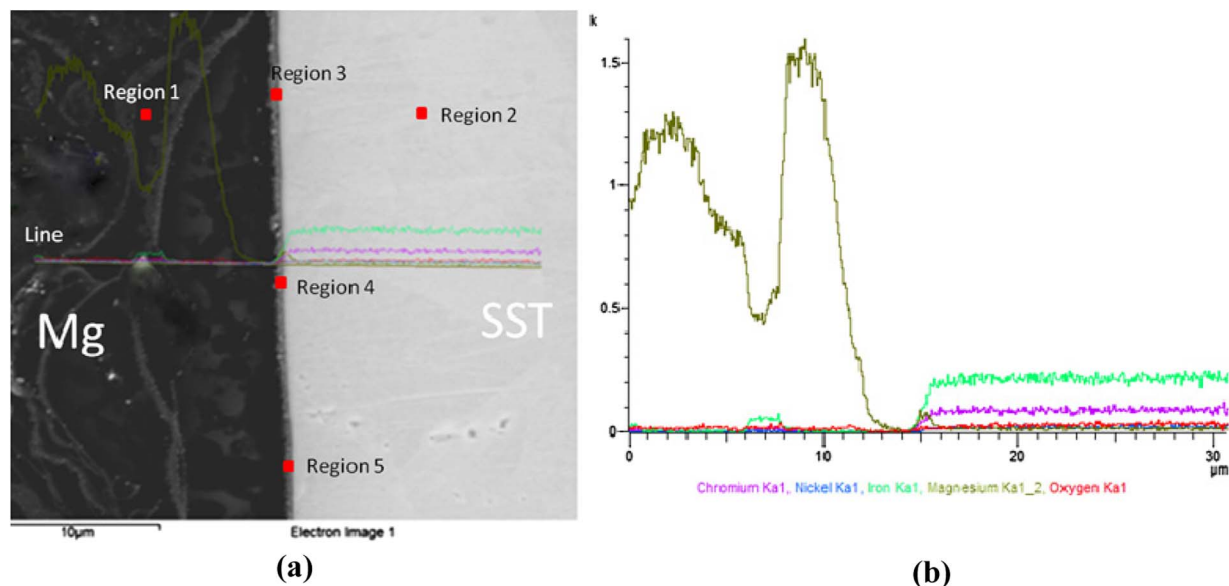


Fig. 9. (a) SEM view of cross section of Mg alloy and SST welding with EDX line and spot analytical region highlighted. (b) EDX line analytical results across the centerline of the welding beam.

Figures 10(a)–10(e) show the typical EDX spot analytical results of regions 1–5 in the cross-section view of Mg–SST (1.5 MHz and 30 W) shown in Fig. 9(a). The element concentrations (both weight percentage and atomic percentage) are shown in the insets. All Mg, Fe, Cr, and Ni exist in the weld fusion zones in regions 3–5. The concentration variations of these elements are very small, indicating uniform mixing of Mg and SST in the welding seam.

As shown in Figs. 9 and 10, an ultra thin reaction layer was clearly visible at the interface of the Mg–SST joint. The layer exhibits a continuous and uniform morphology, where the thickness is approximately 0.5 μm. It was evident that metallurgical bonding rather than mechanical bonding was achieved at the Mg/SST interface.

High bonding strength can be achieved if a thin and uniform compound layer is formed between Mg alloys and steels. Such a compound is possible by a reaction between alloying elements in Mg alloys. For the formation of the thin and uniform compound layer, the nucleation of the compound must occur simultaneously at the whole bonding interface, which is not easily achieved by conventional laser-welding methods.

B. Tensile Testing and Microhardness Measurement

Vickers microhardness was determined by using a load of 100 g using the ASTM 384 and 578 method and a dwell time of 10 s (Mitutoyo MicroMet 5104 HM-122). All the microhardness values presented in this study are averages of three values taken on the same specimen. The center point of the fusion zone was determined carefully after observing the weld geometry under microscope, and all the indentations were adequately spaced to avoid any potential effect of the strain field caused by adjacent indentations. Tensile tests were performed on a fully

computerized tensile testing machine (Shimadzu Autography AG-IS series) at room temperature and with a travel speed of 1.2 mm/min.

Figure 11(a) shows the tensile strength of Al–SST welding for different repetition rates with the same average power (30 W). With increasing repetition rate, the tensile strength increases, and a maximum of 210 MPa tensile strength was observed with repetition rate of 1.5 MHz and 30 W average power. This is in the same range as other dissimilar material welding results using CW or long-pulsed lasers [19–21]. It is important to note that the tensile strength can be enhanced by further optimization of laser parameters (repetition rate, pulse energy, and welding speed).

Figure 11(b) shows the typical microhardness profile across the Al–SST butt welding area with different repetition rates and the same average power (30 W). The hardness of Al is typically lower (60 HV), and a clear trend of continuously increasing hardness from base metals to the welding zone is observed. The microhardness for a lower repetition rate is increased sharply in the welding area and is comparable with CW and ns laser welding (large variation in welding region) [4,22,23]. For CW or ns laser welding, the hardness in and around the joint can help evaluate the brittleness of the weld and whether the weld has the desired strength. The high hardness gives low ductility, which easily causes cracks at the joint. The decrease of microhardness for higher repetition rates indicates the reduction of the intermetallic layer. It is believed that the microhardness can be further reduced when the repetition rate goes up to the gigahertz range.

Figure 12(a) shows the tensile strength of Mg–SST welding for different repetition rates with the same average power (30 W). With increasing repetition rate, the tensile strength increases, and a maximum of 175 MPa tensile strength is observed with

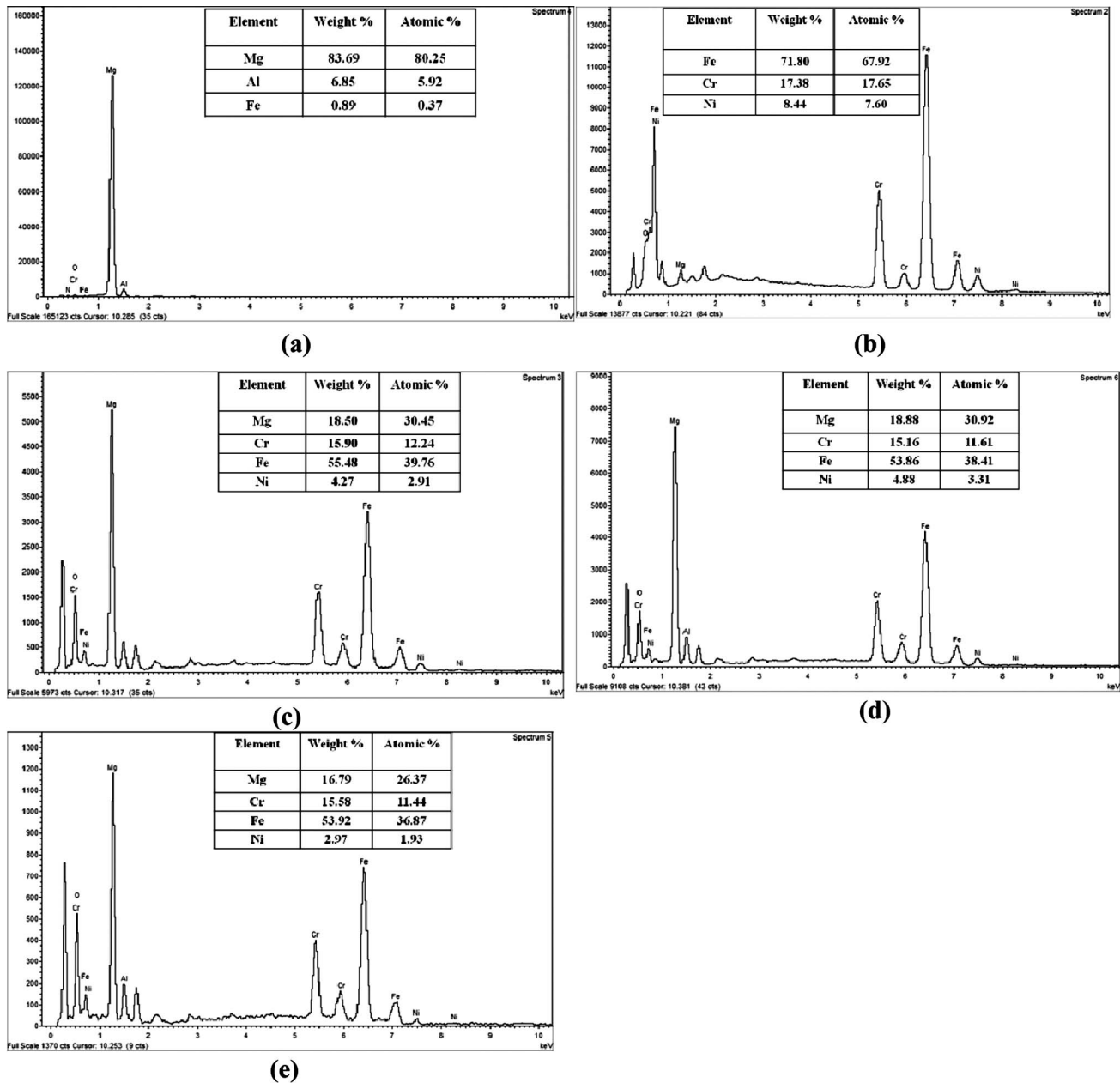


Fig. 10. EDX spot analytical results of different regions in the cross section view of Fig. 9: (a) region 1, pure Mg alloy; (b) region 2, pure SST; (c) region 3; (d) region 4; and (e) region 5.

repetition rate of 1.5 MHz and 30 W average power. Figure 12(b) shows the typical microhardness profile across the Mg–SST butt welding area with different repetition rates and the same average power (30 W). A transition is observed in the welding zone for the microhardness values from Mg base metal to SST base metal. The uniform hardness outside the welding region also demonstrates the absence of HAZ. For welding using CW or ns lasers, the hardness in the HAZ has large variation [24] and can be a weak point of material failure. The size of the microhardness indenter was too large to measure the hardness of the intermetallic layer formed at the interface, so higher hardness values are expected for the laser, as compared with the Al–SST results above.

In order to realize superior laser welding for different materials, it is ideal to integrate laser processing with real-time monitoring of process parameters and characterizing processed results with proper tools. Generally, it is difficult to recognize the point at which a laser action must be discontinued to ensure uniform laser welding. The LIBS method is incorporated in the laser processing, allowing for real-time monitoring of the laser processing parameters and characterizing the processed results by synchronizing with plasma spectrum analysis during the welding process. It can provide real-time manipulation of the laser parameters and performance relative to different processing times and locations.

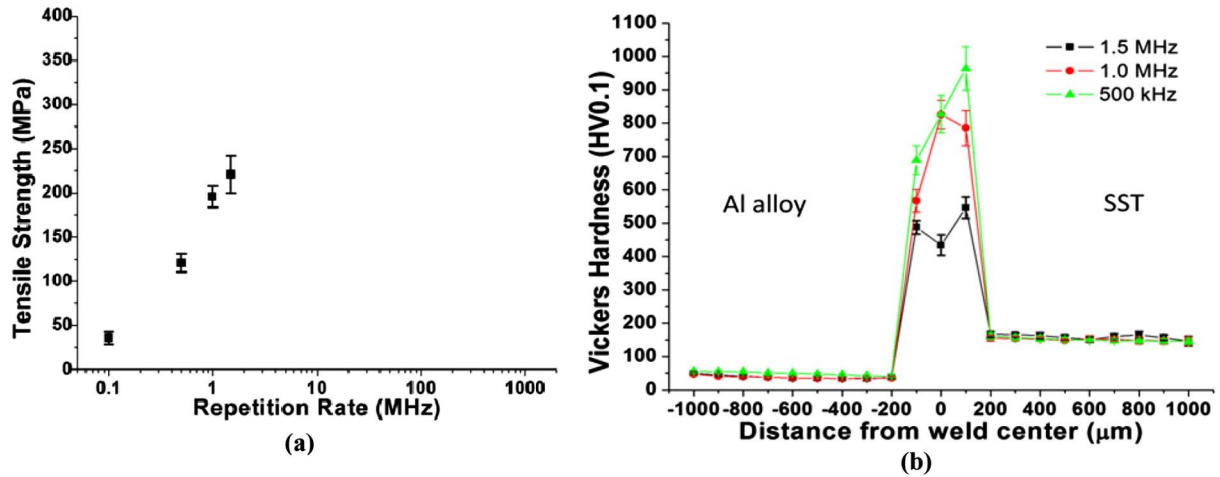


Fig. 11. (a) Tensile strength and (b) microhardness profile of welding zone for Al-SST welding with different repetition rates and the same average power (30 W)

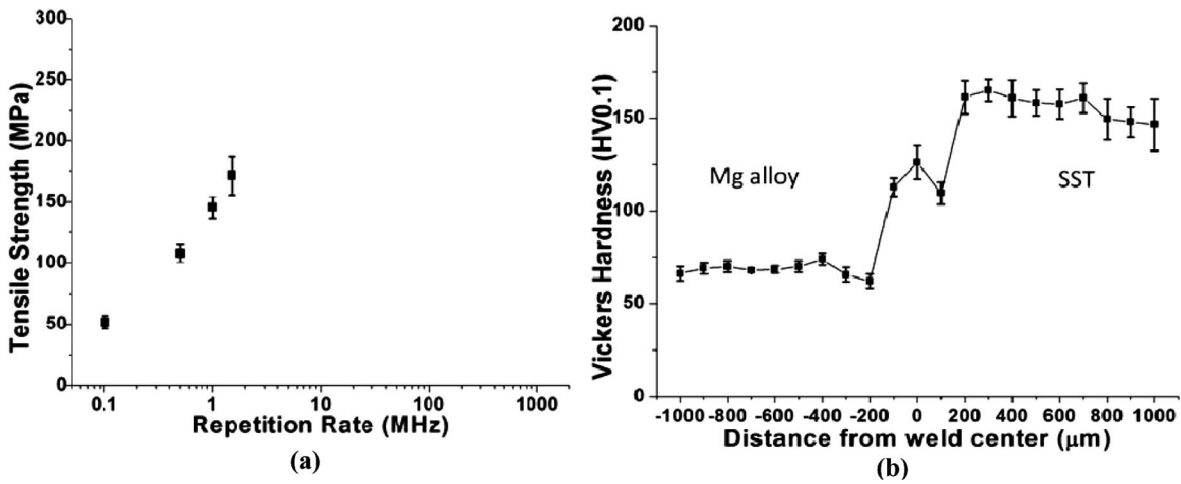


Fig. 12. (a) Tensile strength and (b) microhardness profile of welding zone for Mg-SST welding with different repetition rates and the same average power (30 W)

Figure 13 shows a typical LIBS signal of Mg-SST metal welding. The atomic peak is listed for the atomic peak of Mg and Fe observed in the process

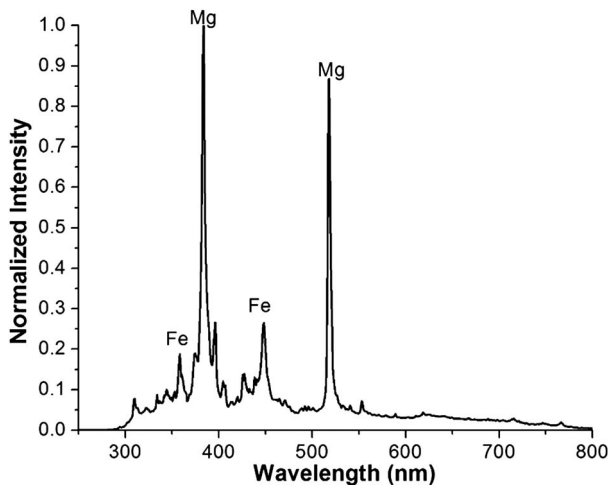


Fig. 13. LIBS signal Mg-SST welding by using fs fiber laser.

of welding. This creates the potential for real-time processing control and monitoring for fs laser welding. During this process, the system can distinguish between nonuniform and uniform welding from the relative peak intensity ratio of the major element of the welded materials.

4. Conclusion and Outlook

Dissimilar metal welding has been experimentally demonstrated using a high-energy high-repetition-rate fs fiber laser. The results show that the formation of intermetallic brittle phases and welding defects could be effectively restricted with the combination of a higher repetition rate and lower pulse energy. Strong welding quality with more than 210 MPa tensile strength for SST-Al and 175 MPa tensile strength for SST-Mg has been demonstrated, and it shows the potential to obtain even higher tensile strength with a higher repetition rate. The welding area is as small as $0.5 \mu\text{m}$, and minimal HAZ is observed. Uniform and homogenous phase transformation in the welding region has been demonstrated.

This laser microwelding technique can be extended for various applications in semiconductor, automobile, aerospace, and biomedical industries.

Future studies include experimental study with repetition rate of gigahertz level with even lower fluence and the influence of welding results with larger focal spot size.

This work was partially supported by DOE, NSF, NIST, and AFOSR.

References

1. X. Cao and M. Jahazi, "Effect of welding speed on butt joint quality of Ti-6Al-4V alloy welded using a high-power Nd:YAG laser," *Opt. Lasers Eng.* **47**, 1231–1241 (2009).
2. C. Barbatti, J. Garcia, G. Liedl, and A. Pyzalla, "Joining of cemented carbides to steel by laser beam welding," *Materialwissenschaft Und Werkstofftechnik* **38**, 907–914 (2007).
3. R. Akhter, L. Ivanchev, and H. Burger, "Effect of pre/post T6 heat treatment on the mechanical properties of laser welded SSM cast A356 aluminium alloy," *Mater. Sci. Eng. A* **447**, 192–196 (2007).
4. T. Mai and A. Spowage, "Characterisation of dissimilar joints in laser welding of steel–kovar, copper–steel and copper–aluminium," *Mater. Sci. Eng. A* **374**, 224–233 (2004).
5. H.-C. Chen, A. J. Pinkerton, and L. Li, "Fibre laser welding of dissimilar alloys of Ti-6Al-4V and Inconel 718 for aerospace applications," *Int. J. Adv. Manuf. Technol.* **52**, 977–987 (2011).
6. R. Borrisutthekul, T. Yachi, Y. Miyashita, and Y. Mutoh, "Suppression of intermetallic reaction layer formation by controlling heat flow in dissimilar joining of steel and aluminum alloy," *Mater. Sci. Eng. A* **467**, 108–113 (2007).
7. Y. Ozeki, T. Inoue, T. Tamaki, H. Yamaguchi, S. Onda, W. Watanabe, T. Sano, S. Nishiuchi, A. Hirose, and K. Itoh, "Direct welding between copper and glass substrates with femtosecond laser pulses," *Appl. Phys. Express* **1**, 082601 (2008).
8. W. Watanabe, S. Onda, T. Tamaki, K. Itoh, and J. Nishii, "Space-selective laser joining of dissimilar transparent materials using femtosecond laser pulses," *Appl. Phys. Lett.* **89**, 021106 (2006).
9. K. Kim and Z. Guo, "Ultrafast radiation heat transfer in laser tissue welding and soldering," *Numer. Heat Transfer Part A Applications* **46**, 23–40 (2004).
10. S. M. Eaton, H. Zhang, M. L. Ng, J. Li, W.-J. Chen, S. Ho, and P. R. Herman, "Transition from thermal diffusion to heat accumulation in high repetition rate femtosecond laser writing of buried optical waveguides," *Opt. Express* **16**, 9443–9458 (2008).
11. S. Richter, S. Döring, A. Tünnermann, and S. Nolte, "Bonding of glass with femtosecond laser pulses at high repetition rates," *Appl. Phys. A* **103**, 257–261 (2011).
12. D. Lee and E. Kannatey-Asibu, "Numerical analysis on the feasibility of laser microwelding of metals by femtosecond laser pulses using ABAQUS," *J. Manuf. Sci. Eng.* **130**, 061014 (2008).
13. J. Huang, Y. Zhang, and J. Chen, "Ultrafast solid–liquid–vapor phase change in a thin gold film irradiated by multiple femtosecond laser pulses," *Int. J. Heat Mass Transfer* **52**, 3091–3100 (2009).
14. P. Wan, L. Yang, and J. Liu, "All fiber-based Yb-doped high energy, high power femtosecond fiber lasers," *Opt. Express* **21**, 29854–29859 (2013).
15. J. Ma, M. Harooni, B. Carlson, and R. Kovacevic, "Dissimilar joining of galvanized high-strength steel to aluminum alloy in a zero-gap lap joint configuration by two-pass laser welding," *Mater. Des.* **58**, 390–401 (2014).
16. H. Laukant, C. Wallmann, M. Müller, M. Korte, B. Stirn, H.-G. Haldenwanger, and U. Glatzel, "Fluxless laser beam joining of aluminium with zinc coated steel," *Sci. Technol. Weld. Joining* **10**, 219–226 (2005).
17. L. Li, C. Tan, Y. Chen, W. Guo, and F. Song, "Comparative study on microstructure and mechanical properties of laser welded–brazed Mg/mild steel and Mg/stainless steel joints," *Mater. Des.* **43**, 59–65 (2013).
18. L. Li, C. Tan, Y. Chen, W. Guo, and C. Mei, "CO₂ laser welding–brazing characteristics of dissimilar metals AZ31B Mg alloy to Zn coated dual phase steel with Mg based filler," *J. Mater. Process. Technol.* **213**, 361–375 (2013).
19. M. Rathod and M. Kutsuna, "Joining of aluminum alloy 5052 and low-carbon steel by laser roll welding," *Weld. J.* **83**, 16-S–26-S (2004).
20. M. Gao, C. Chen, Y. Gu, and X. Zeng, "Microstructure and tensile behavior of laser arc hybrid welded dissimilar Al and Ti alloys," *Materials* **7**, 1590–1602 (2014).
21. S.-J. Lee, H. Nakamura, Y. Kawahito, and S. Katayama, "Microstructural characteristics and mechanical properties of single-mode fiber laser lap-welded joint in Ti and Al dissimilar metals," *Trans. JWRI* **42**, 17–21 (2013).
22. G. Mirshekari, A. Saatchi, A. Kermanpur, and S. Sadrnezhad, "Laser welding of NiTi shape memory alloy: comparison of the similar and dissimilar joints to AISI 304 stainless steel," *Opt. Laser Technol.* **54**, 151–158 (2013).
23. A. Mathieu, R. Shabadi, A. Deschamps, M. Suery, S. Mattei, D. Grevey, and E. Cicala, "Dissimilar material joining using laser (aluminum to steel using zinc-based filler wire)," *Opt. Laser Technol.* **39**, 652–661 (2007).
24. X. Cao, M. Jahazi, J. Immarigeon, and W. Wallace, "A review of laser welding techniques for magnesium alloys," *J. Mater. Process. Technol.* **171**, 188–204 (2006).